P12

HAS3: A radiation tolerant CMOS image sensor for space applications

Manuel Innocent, Thomas Cools, Carl Luypaert, Cedric Esquenet, Stefan Janssens, Wiet Vroom, Joris De Bondt*, Ishwar Chandra Mudegowdar, Patrick Pintens, Peter Deruytere*, Dirk Van Aken*, Ioannis Thanasopoulos, Joost Decupere and Tomas Geurts

ON Semiconductor, Schaliënhoevedreef 20B, 2800 Mechelen, Belgium.
Manuel.Innocent@onsemi.com, tel +32 15 446 390

This paper presents the design and characterization of a radiation tolerant sensor for space applications. The sensor is optimized to withstand both long term degradation due to radiation and instantaneous single event effects that could lead to a functional interrupt.

The main long term degradation effect is an increase of the dark current of the photo diode due to ionizing dose and displacement damage. The results of pixel layout and process optimization experiments were previously reported [1, 2]. This paper describes the design approach to mitigate single event effects and shows characterization data from the final product.

Motivation

The presented radiation tolerant sensor is a next step in the long tradition of radiation tolerant image sensor designs developed at ON semiconductor. The sensor is designed for the European Space Agency (ESA) and it is targeted at Attitude and Orbit Control Systems (AOCS), commonly known as "star trackers". The sensor has additional operating modes that also make it suitable for video applications like e.g. docking cameras for space crafts.

Sensor design

The sensor has 1280x1280 5T pixels at an 11µm pitch and supports both rolling shutter and pipelined global shutter. The main operating mode is rolling shutter readout at 10 fps, but the sensor supports frame rates up to 60 fps. The sensor has 12-bit column-parallel delta-sigma [3,4,5,6] A/D converters. The block diagram of the sensor is shown in figure 1 and the key specifications are summarized in table 1.

To minimize the power consumption in its nominal operating mode, the sensor supports a windowing mode where only selected regions of the image are read out and the unused ADC's are power down. The power control is in blocks of 32 ADC's and the pattern can be changed at line rate.

The sensor is designed in a conventional 180nm CMOS image sensor process using a normal standard cell library. The main customer requirement with respect to single event effects for this sensor is that it is acceptable to lose a single pixel, a corrupt line should be an unlikely event and losing a complete frame is unacceptable. This is guaranteed by taking multiple precautions in the design [7].

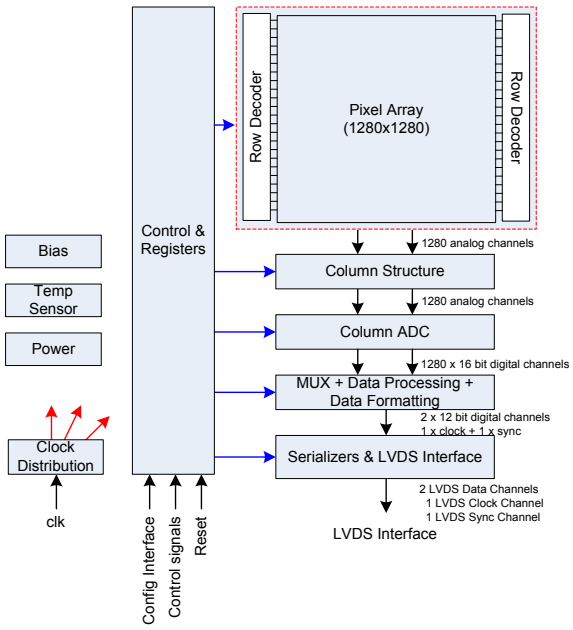

Figure 1: Block diagram of the HAS3 sensor

Single event effect mitigation

"The functional operating modes are hardwired predefined modes that cannot be corrupted at all. User defined evaluation modes are stored in triple redundant registers."

The functional operating modes are the modes for the main application of the sensor: star tracking. All these modes run at 10 fps. They trade additional functionality (e.g. triple redundant A/D conversions) for power consumption. Except for these modes, the sensor also has an evaluation mode where it can be configured by register uploads. Although all settings are stored in triple redundant registers, this mode is considered less safe in critical applications. In evaluation mode the frame rate of the sensor can be increased up to 60 fps which allows for video applications. Figure 2 shows the block diagram of a configuration register. Depending on external control signals, the configuration is read from one of the predefined sets or from registers.

* Previously with ON Semiconductor

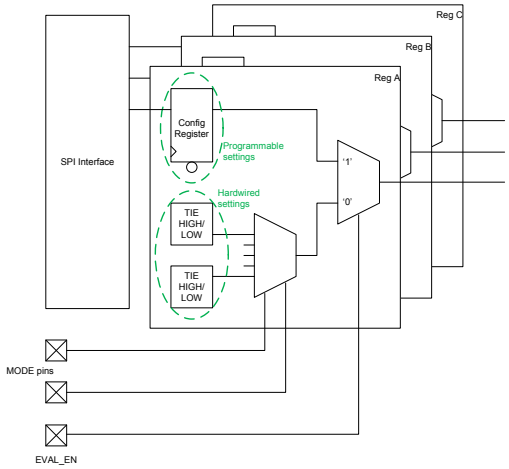

Figure 2: Predefined Hardwired operating modes

"Triple mode redundant (TMR) logic with triple phase skewed clock trees guarantee that state machines on the control path won't lose their state."

All logic on the control path (e.g. ADC controller) uses triple redundant flip-flops. Each of the three flip-flops of a cell is clocked from a different clock tree and the three clocks have a small delay relative to each other. This allows having only a single instance of the combinatorial logic since any disruption of the logic by a particle will only last for a short time. It is unlikely that two flip-flops would sample the wrong signal at different times. In case one of the clocks is disrupted only one of the three flip-flops would sample the data at the wrong time. Spatially, the flip-flops of a cell are separated by at least 60 µm. This distance is enough so that a single hit by a particle would not disrupt more than one flip-flop of the cell.
The data path does not use TMR logic since the area and power penalty would be too large and in case of a disruption only a single pixel value is affected.

"A triple A/D conversion mode with median filtering reduces susceptibility of the sensor to e.g. solar flares."

At times of high particle flux, the risk of corrupted A/D conversions is minimized by the triple conversion mode where the output is the median of three consecutive conversions of the same signal. This is an alternative to having TMR logic on the data path. It does not affect the nominal frame rate. It does however increase the power consumption of the sensor.

"An external controller minimizes risks and maximizes flexibility for the user."

An external controller is a desired feature in this market segment. It allows instrument manufacturers to optimize the sensor timing and it also completely eliminates the risk of a functional interrupt of the controller due to an SEE. It shifts the responsibility for the stability of the controller to the system level. Since the digital data path is on the sensor, the controls are not limited to the typical image sensor controls. The controller also has to indicate the datatype of an A/D conversion to define the required data path operations for e.g. CDS and calibration.

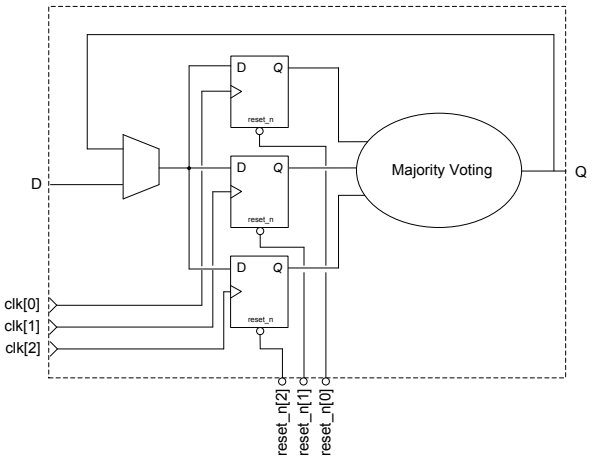

Figure 3: TMR memory cell with Redundant Clock and Reset Trees. The output of the cell is the result of majority voting on the flip-flop outputs.

Table 1: key specifications

Parameter	**Specification**
Resolution	1280 x 1280
Pixel Size	11 µm x 11µm
Pixel Type	Radiation Tolerant 5T
Shutter Type	Rolling Shutter, Pipelined Global Shutter
Temporal Noise	30 e-
Full Well Charge	70,000 e-
QE	45% at 550 nm
Dark Signal	< 20e^-/s @ 22°C BOL <700 e^-/s @ 22°C EOL (spec)
Frame Rate	10 fps nominal, 60 fps max
Master Clock	192 MHz
Windowing Features	Capable of supporting multiple windowing with reduction in power consumption
ADC Resolution	12 bit ENOB
Output Interface	LVDS/subLVDS
Data Rate	4 LVDS x 384 Mbps
Power Consumption	400 mW @ 10fps for 2 data outputs
Package	88-pin Hermetically Sealed CQFP
Total Dose EOL	50Krad 1.8E10p/cm2@10MeV
SEL/SEFI	105 MeVcm^2/mg with tilted angle (target, still under evaluation)

Characterization

The sensor is characterized for both electro-optical performance and radiation tolerance [8, 9, 10, 11]. Since the electro-optical characterization does not show anything unexpected and ionizing dose did not show any issues on the test chip, the focus of this paper is on high energetic proton radiation (displacement damage) and heavy ions (single event effects).

Figures 4 to 7 show the post radiation dark current as a function of proton fluence and anneal conditions for two proton energies. This data is measured within an hour after radiation. Contrary to what was observed on the test chip [1,2], the dark current does scale as would be expected by the NIEL difference [12].

The data presented in [1,2] showed an 8x higher dark current after radiation with 14.4 MeV protons versus radiation with 62 MeV protons, while based on the NIEL difference between those energies a factor of 2x is expected. The origin of this discrepancy is suspected to be in the way the 14.4 MeV proton beam is generated at the cyclotron. The lower energies are generated by placing degraders (polyethylene blocks) in the 62 MeV beam. To go down to 14.4 MeV requires a large number of degraders in series in the beam. This results in a high uncertainty on the output spectrum. It was suspected the output spectrum has some lower energy component which has a very high NIEL. This contribution is assumed to corrupt the measurement. Since this is fundamental to the way the lower energy protons are generated at the facility we worked with, only higher energies were used for the new measurements. At 30 MeV and 58 MeV the data is much more consistent with the factor 1.4x expected based on the NIEL difference between these energies.

Driven by the test chip results, the sensor is manufactured on three different EPI resistivity levels. Based on the post proton radiation dark current the 5 Ωcm is clearly preferred. Figure 7 show the annealing of three samples that where radiated slightly beyond EOL conditions. The dark current anneals quite well over time since it reduces by a factor 2 over a period of a few months.

An initial heavy ion radiation experiment was done on a very small number of devices. The experiment uses the three heaviest ions available at the cyclotron: Ni, Kr and Xe. The main purpose of this initial experiment is optimizing our procedure based on the ESA guidelines [13]. Figure 8 shows an example of an image grabbed during radiation with Xe ions. The diameter of the area affected by a Xe hit is slightly over 60 µm. This is consistent with the choice of the minimum distance between the flip-flops in the digital design. More elaborate experiments are planned.

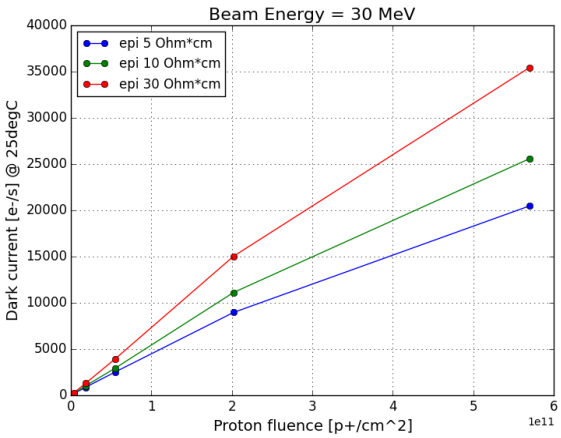

Figure 4: Post radiation dark current as a function of proton fluence for 30 MeV protons with epi resistivity as a parameter.

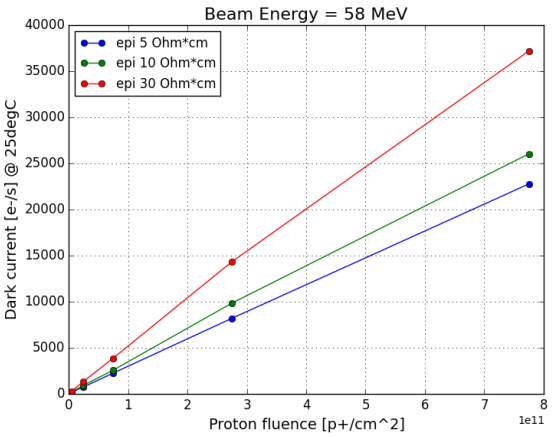

Figure 5: Post radiation dark current as a function of proton fluence for 58 MeV protons with epi resistivity as a parameter

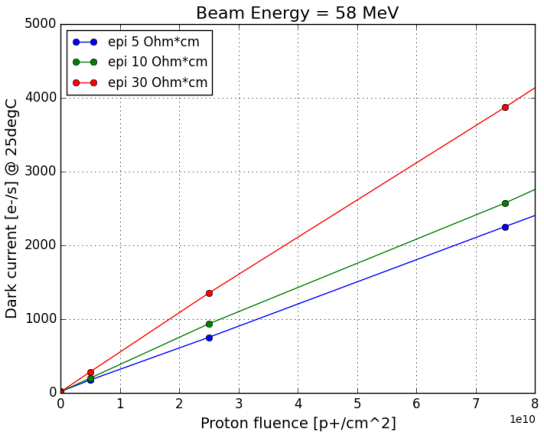

Figure 6: Post radiation dark current as a function of proton fluence for 58 MeV protons with epi resistivity as a parameter. Zoom on the region around the sensor EOL specification. The EOL specification is equivalent to 4.25 p^+/cm^2 at 58 MeV

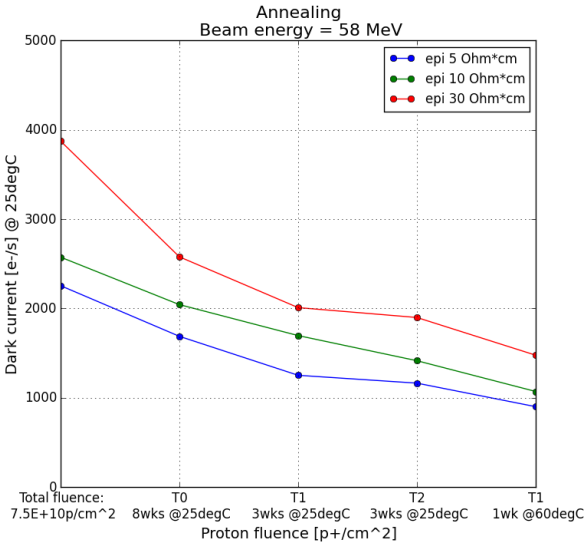

Figure 7: Post radiation dark current as a function of anneal time and conditions for 58 MeV protons with epi resistivity as a parameter. Room temperature anneal reduces the dark current by 2X after a few months. This allows meeting the EOL dark current specification in real life conditions

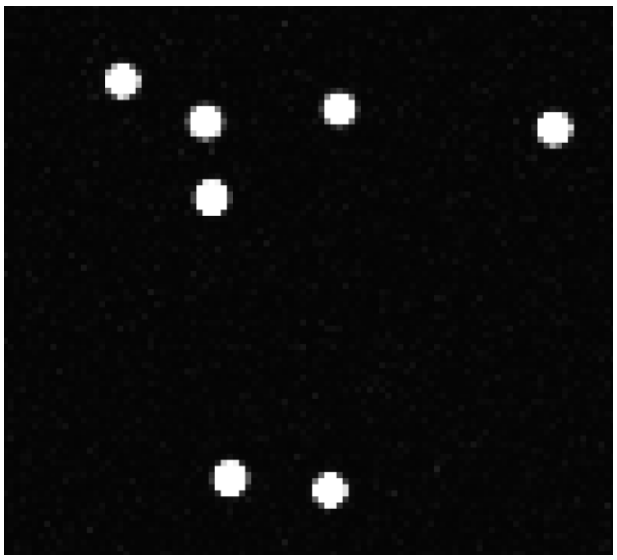

Figure 8: Small region of an image grabbed during radiation with Xe. The area that is affected by one hit is roughly limited to 6x6 pixels. The pixel pitch is 11 µm, so the diameter of the affected region is slightly over 60 µm. In case of Ni, the affected area is slightly smaller and limited to 5x5 pixels.

Package

The package is a custom designed hermetically sealed ceramic quad flat pack. Figure 9 shows a picture of a sensor. Full hermetic sealing is desired to prevent moisture penetrating in the package before launch. The package is designed to facilitate the assembly and inspection in the instrument. The top of the ceramic (dark area next to the gold colored seal ring) is the reference plane of the sensor. This is convenient for alignment of the sensor in the instrument since thickness variations of the ceramic do not matter. The leads can be bent a little during assembly to avoid thermal induced stress on the connections later on. The leads provide both thermal and mechanical separation between the optical system and the electronics. Visual inspection of the assembled part is easy since the soldered leads are next to the sensor and the bond wires can be seen through the sensor cover glass.

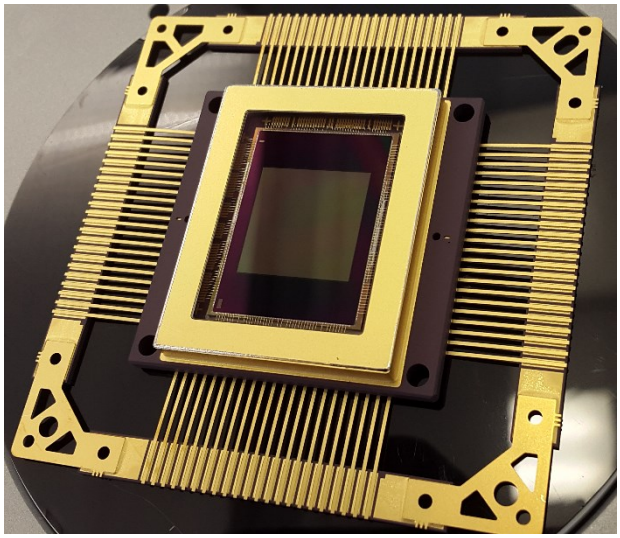

Figure 9: Packaged HAS3 sensor. The leads of the ceramic quad flat pack are connected to a ring that prevents damage. This ring is removed when the sensor is assembled in the instrument.

Conclusion

This paper presents a sensor optimized for space applications. The optimization of the pixel layout and process were previously reported. This paper presents new data on the dark current increase due to displacement damage which was identified earlier as a critical issue. The new data confirms that the sensor meets the specification when taking annealing into account. The paper also discusses the design approach taken to mitigate single event effects. However, the evaluation of the sensor under heavy ion radiation is still ongoing at this time.

References

[1] M. Innocent, “A Radiation Tolerant 4T pixel for Space Applications: Layout and Process Optimization,” in Proc. IISW 2013.

[2] M. Innocent, “A radiation tolerant 4T pixel for space applications: layout and process optimization” Workshop on CMOS Image Sensors for High Performance Applications. Toulouse 26, 27 Nov 2013.

[3] Z. Zhou, B. Pain, R. Panicacci, B. Mansoorian, J. Nakamura, and E.R. Fossum, “On-focal-plane ADC: Recent progress in on-focal plane ADCs”, 1996, Infrared Readout Electronics III, Proc. SPIE vol. 2745, pp. 111-122

[4] Y. Chae et al., "A 2.1 M Pixels, 120 Frame/s CMOS Image Sensor With Column-Parallel ADC Architecture," 2011, IEEE Journal of Solid-State Circuits, vol. 46, no. 1, pp. 236-247

[5] A. Xhakoni, G. Gielen, “Designing Incremental Sigma-Delta ADCs for Low Thermal Noise in Image Sensors”, 2013, International Image Sensor Workshop (IISW)

[6] B. Cremers et al., “A 5 Megapixel, 1000fps CMOS Image Sensor with High Dynamic Range and 14-bit A/D Convertors”, 2013, International Image Sensor Workshop (IISW)

[7] R. Weigand, “Single Event Effect Mitigation in Digital Integrated Circuits for Space”, 2010, Topical Workshop on Electronics for Particle Physics, Aachen, Germany

[8] V. Goiffon et al., “Radiation Effects in Pinned Photodiode CMOS Image Sensors: Pixel Performance Degradation Due to Total Ionizing Dose,” IEEE Trans. Nucl. Sci., vol. 59, pp. 2878–2887, Dec. 2012.

[9] C. Virmontois, V. Goiffon, F. Corbière, P. Magnan, S. Girard, and A.Bardoux, “Displacement Damage Effects in Pinned Photodiode CMOS Image Sensors,” IEEE Trans. Nucl. Sci., vol. 59, pp. 2872–2877, Dec. 2012.

[10] Jan Bogaerts, Bart Dierickx, Guy Meynants, and Dirk Uwaerts, “Total Dose and Displacement Damage Effects in a Radiation-Hardened CMOS APS,” IEEE Trans. Nucl. Sci., vol. 50, pp. 84–90, Jan. 2003.

[11] Padmakumar R. Rao, Xinyang Wang, Adri J. Mierop, and Albert J.P. Theuwissen, “Gamma-Ray Irradiation Effects on CMOS Image Sensors in Deep Sub-Micron Technology,” in Proc. IISW, 2007.

[12] J. R. Srour and D. H. Lo, “Universal damage factor for radiation-in-duced dark current in silicon devices,” IEEE Trans. Nucl. Sci., vol. 47, no. 6, pp. 2451–2459, Dec. 2000.

[13] ESA, “Single Event Effects Test Method and Guidelines,” ESCC Basic Specification No. 25100 Issue 2. https://escies.org/download/specdraftapppub?id=3095